Acta Pharmacologica Sinica

www.nature.com/aps

ARTICLE

Aminoacylase-1 plays a key role in myocardial fibrosis and the therapeutic effects of 20(*S*)-ginsenoside Rg3 in mouse heart failure

Qiong Lai[1], Fu-ming Liu[2], Wang-lin Rao[1], Guang-ying Yuan[1], Zhao-yang Fan[1], Lu Zhang[1], Fei Fu[1], Jun-ping Kou[1], Bo-yang Yu[1] and Fang Li[1]

We previously found that the levels of metabolite *N*-acetylglutamine were significantly increased in urine samples of patients with heart failure (HF) and in coronary artery ligation (CAL)-induced HF mice, whereas the expression of its specific metabolic-degrading enzyme aminoacylase-1 (ACY1) was markedly decreased. In the current study, we investigated the role of ACY1 in the pathogenesis of HF and the therapeutic effects of 20(*S*)-ginsenoside Rg3 in HF experimental models in vivo and in vitro. HF was induced in mice by CAL. The mice were administered Rg3 (7.5, 15, 30 $mg \cdot kg^{-1} \cdot d^{-1}$, i.g.), or positive drug metoprolol (Met, 5.14 $mg \cdot kg^{-1} \cdot d^{-1}$, i.g.), or ACY1 inhibitor mono-tert-butyl malonate (MTBM, 5 $mg \cdot kg^{-1} \cdot d^{-1}$, i.p.) for 14 days. We showed that administration of MTBM significantly exacerbated CAL-induced myocardial injury, aggravated cardiac dysfunction, and pathological damages, and promoted myocardial fibrosis in CAL mice. In Ang II-induced mouse cardiac fibroblasts (MCFs) model, overexpression of ACY1 suppressed the expression of COL3A1 and COL1A via inhibiting TGF-β1/Smad3 pathway, whereas ACY1-siRNA promoted the cardiac fibrosis responses. We showed that a high dose of Rg3 (30 $mg \cdot kg^{-1} \cdot d^{-1}$) significantly decreased the content of *N*-acetylglutamine, increased the expression of ACY1, and inhibited TGF-β1/Smad3 pathway in CAL mice; Rg3 (25 μM) exerted similar effects in Ang II-treated MCFs. Meanwhile, Rg3 treatment ameliorated cardiac function and pathological features, and it also attenuated myocardial fibrosis in vivo and in vitro. In Ang II-treated MCFs, the effects of Rg3 on collagen deposition and TGF-β1/Smad3 pathway were slightly enhanced by overexpression of ACY1, whereas ACY1 siRNA partially weakened the beneficial effects of Rg3, suggesting that Rg3 might suppress myocardial fibrosis through ACY1. Our study demonstrates that *N*-acetylglutamine may be a potential biomarker of HF and its specific metabolic-degrading enzyme ACY1 could be a potential therapeutic target for the prevention and treatment of myocardial fibrosis during the development of HF. Rg3 attenuates myocardial fibrosis to ameliorate HF through increasing ACY1 expression and inhibiting TGF-β1/Smad3 pathway, which provides some references for further development of anti-fibrotic drugs for HF.

Keywords: heart failure; myocardial fibrosis; *N*-acetylglutamine; aminoacylase-1; 20(*S*)-ginsenoside Rg3; targeted metabolomics analysis

Acta Pharmacologica Sinica (2022) 43:2003–2015; https://doi.org/10.1038/s41401-021-00830-1

INTRODUCTION

Heart failure (HF) is the final stage of multiple cardiovascular diseases with high mortality [1]. HF is caused by myocardial damage and changes in the structure and function of myocardium, and finally leads to low ventricular filling function or pump blood, in which fibrosis becomes a key contributor to tissue stiffness and dysfunction [2]. The conventional therapeutic approaches in HF management are diuretics, angiotensin-converting enzyme inhibitors, angiotensin receptor blockers, β-blockers, and the like [3]. However, it is still insufficient to reduce rehospitalization rates and mortality due to that myocardial fibrosis persists even when treated as recommended by the official guidelines [4, 5]. Therefore, exploring the underlying pathological mechanisms of myocardial fibrosis and developing novel therapeutic drugs are needed to enhance the survival and life quality in HF patients.

Current researches have elucidated that myocardial fibrosis is mainly characterized by the adverse accumulation of collagen and other extracellular matrices [6]. Numerous evidence indicates that transforming growth factor-beta (TGF-β) is the central regulator of fibrosis across many organ types and TGF-β1/smad family member 3 (Smad3) signaling pathway exerts a critical role in the development of myocardial fibrosis [7, 8]. Whereas, treatment strategy based on direct TGF-β regulation has led to many side effects and there are almost no effective means to reverse myocardial fibrosis [9, 10]. Hence, it is critical to find a safer and

[1]Jiangsu Key Laboratory of TCM Evaluation and Translational Research, Research Center for Traceability and Standardization of TCMs, School of Traditional Chinese Pharmacy, China Pharmaceutical University, Nanjing 211198, China and [2]Jiangsu Province Hospital of Chinese Medicine, Affiliated Hospital of Nanjing University of Chinese Medicine, Nanjing 210029, China
Correspondence: Bo-yang Yu (boyangyu59@163.com) or Fang Li (lifangcpu@163.com)

Received: 7 September 2021 Accepted: 21 November 2021
Published online: 16 December 2021

more effective therapeutic target for myocardial fibrosis in HF. Recently, metabolite has generated lots of interest among researchers because of its involvement in different human diseases [11, 12], and metabolic alterations are also recognized as the important pathogenic process of fibrosis. The combination of metabolomics and molecular biology might be the important approach to reveal the underlying pathological mechanisms of myocardial fibrosis and offer new therapeutic targets for myocardial fibrosis to improve HF.

Panax ginseng C.A. Meyer (Araliaceae), a representative traditional Chinese medicine for cardiovascular disease, has been most widely studied as a suitable candidate in the treatment of HF [13, 14]. The pharmacological efficacy and mechanisms of ginseng are closely associated with ginsenosides [15]. Ginsenoside Rg3 (Rg3) is one of the major active components in ginseng and exhibits obvious therapeutic effects on cardiovascular diseases [16, 17]. However, the effect of Rg3 on HF remains to be elucidated. In addition, previous studies reported that Rg3 could exert hepatic fibrosis improvement through regulating inflammation-mediated autophagy and inhibit keloid fibroblast proliferation via ERK signaling pathways [18, 19]. Although the potential of Rg3 to ameliorate myocardial fibrosis remains obscure. Therefore, the effect and mechanism of Rg3 on myocardial fibrosis are worthy of further studies in view of its possible development as adjunctive therapy to existing medications in the treatment of HF. In agreement with the holistic thinking of TCM, different metabolomic technologies recently have been applied to evaluate the efficacy and biochemical action mechanism of TCM [20], as well as treatments of different diseases such as cardiovascular disease [21], kidney disease [22–24], liver disease [25], and metabolic disease [26]. In view of this, metabonomics technology is also a good way to clarify the effect and mechanism of Rg3 on myocardial fibrosis and HF.

In our previous work, metabolite *N*-acetylglutamine has been found to significantly increase in the urine of HF mice by using untargeted metabolomics, and the transcriptomic results also showed that the expression of its specific metabolic-degrading enzyme aminoacylase-1 (ACY1) gene decreased abnormally in the heart tissues of HF mice [27]. Nevertheless, the specific role of *N*-acetylglutamine and ACY1 in HF is still unclear. Thus, this study was designed to reveal its function and involved pathological mechanisms in HF and further explore the effect and mechanism of Rg3 on HF aimed to develop novel therapeutic targets in HF and enrich the clinical application basis of Rg3.

MATERIALS AND METHODS

Reagents

The ACY1-plasmid and ACY1-siRNA were obtained from Genomeditech (Shanghai, China) Co., Ltd. The information of antibodies and chemicals was shown in Supplementary Table S1.

Human samples

A total of 20 patients with HF and 30 healthy controls from the Jiangsu Province Hospital of Chinese Medicine have been enrolled in the study. Informed consent was obtained from all patients and the study was performed under the guidance of the Declaration of Helsinki. This study was approved by the Ethical Committee (no. 2019NL-089-02). The urine samples were collected and stored at −80 °C for metabolite analysis.

Animal models and drug intervention

Male C57BL/6 J mice (22–25 g) were purchased from Qing Long Shan Dong Wu Fan Zhi Chang (Nangjing, China). The mice were randomly divided into several cages and housed in a standard vivarium with free access to food and water. All procedures were conducted following the National Institutes of Health Guidelines for the Care and Use of Laboratory Animals, and the protocols used were approved by the Animal Ethics Committee of China Pharmaceutical University, Nanjing, China.

The HF mice model was generated by coronary artery ligation (CAL) [28]. The mice were anesthetized with sodium pentobarbital (50 mg/kg) intraperitoneally (i.p.). The slipknot was tied around the left anterior descending coronary artery 3–4 mm from its origin with a 6–0 silk suture for 14 days to induce the HF model. And the same surgical procedures without ligating the left anterior descending coronary artery were performed on sham-operated mice. In addition, metoprolol (Met) is an FDA-approved and common clinical medicine used in the treatment of myocardial ischemia and myocardial infarction [29], and it is often used as a positive drug in basic researches as well [30–32]. Therefore, it was selected as a positive drug in this study. All the mice were monitored for 24 h after the surgery and the survival mice were randomly assigned to two independent sets of experiments as follows:

The survival mice were randomly divided into five groups ($n = 6$/group): Sham group, Model group, Sham+Mono-tert-butyl malonate (MTBM) group, Model+MTBM group, and Met group. In the Sham and Model groups, the mice received an intraperitoneal injection of normal saline every day (Day 1–14). In the Sham+MTBM and Model +MTBM groups, the mice received an intraperitoneal injection of MTBM at a dose of 5 mg/kg every day (Day 1–14). In the Met group, the mice were treated with Met via intragastric administration at a dose of 5.14 mg/kg every day (Day 1–14). All the mice were killed by cervical dislocation to explore the contents of *N*-acetylglutamine in HF and the effects of ACY1 on HF.

The survival mice were randomly divided into six groups ($n = 9$/group): Sham group, Model group, Rg3 (7.5 mg/kg) group, Rg3 (15 mg/kg) group, Rg3 (30 mg/kg) group, and Met group. In the Sham and Model groups, the mice were treated with normal saline in equivalency via intragastric administration every day (Day 1–14). In the Rg3 groups, the mice were treated with 20(*S*)-ginsenoside Rg3 in equivalency and different dosages via intragastric administration every day (Day 1–14). In the Met group, the mice were treated with Met via intragastric administration at a dose of 5.14 mg/kg every day (Day 1–14). All the mice were killed by cervical dislocation to explore the effects and mechanisms of 20(*S*)-ginsenoside Rg3 on HF and myocardial fibrosis.

Targeted metabolomics analysis

Standard stock preparation. Standard stock solutions of ketoprofen and *N*-acetylglutamine were obtained by dissolving each compound separately in methanol and stored at −20 °C. The desired concentrations of ketoprofen and *N*-acetylglutamine were prepared by the dilution of standard stock solutions with methanol.

Sample pretreatment. The mouse urine samples were collected and immediately frozen at −80 °C on the 14th day after CAL. Human urine samples and mouse urine samples were processed as follows. Each urine sample was thawed at room temperature. Ketoprofen solution (10 μL, 4 μg/mL) and 140 μL of methanol were added to 50 μL of urine, then vortex-mixed (1 min) and centrifuged (10 min, 4 °C) at 13,000 r/min to precipitate the proteins. The supernatant was centrifuged for 20 min under the same conditions and filtered through a 0.22 μm pore membrane before analysis.

HPLC-QqQ-MS analysis. Samples were analyzed by the Agilent HPLC-QqQ-MS system (Agilent Technologies Inc, Santa Clara, CA, USA). Analyses were accomplished on a TSK-GEL Amide-80 (150 mm × 2.0 mm i.d., 5 μm) column at a flow rate of 0.20 mL/min. The sample injection volume was 10 μL. The column temperature was maintained at 25 °C. The mobile phase was composed of water containing 0.1% formic acid (A) and acetonitrile containing 0.1% formic acid (B). The gradient elution program began with 95%–85% B

at 0–3 min, 85%–75% B at 3–9 min, 75%–60% B at 9–12 min, 60%–50% B at 12–15 min, 50% B at 15–20 min, and finally back to initial conditions, with 5 min for equilibration. Quantitative analysis of *N*-acetylglutamine was performed using multiple reaction monitoring acquisition modes with *m/z* 189.1 → 130.1 with a scan time of 1.2 s per transition in positive ion mode. The capillary voltage, nozzle voltage, auxiliary gas temperature, auxiliary gas flow rate, sheath gas temperature, sheath gas flow rate, nebulizer gas pressure, collision energy, and fragmented voltage were set at 3500 V, 1500 V, 350 °C, 10 L/min, 350 °C, 12 L/min, 50 psi, 5 V, 105 V, respectively. Data acquisition and processing were performed using Masshunter software. The method was validated for linearity, precision, accuracy, and extraction recovery shown in Supplementary Figure S1 and Supplementary Table S2.

RNA-seq and genome-wide transcriptome analysis

The specific operation process of transcriptome analysis was performed as previously described [33]. In brief, TRIzol (Invitrogen, Los Angeles, CA, USA) was used to isolate the total RNA from fresh ventricular tissue, and then mRNA was purified from total RNA using poly-T oligo-attached magnetic beads. NEBNext® UltraTM RNA Library Prep Kit for Illumina® (NEB, USA) was applied to generate the sequencing libraries according to the manufacturer's recommendations and add index codes to attribute sequences to each sample. The clustering of the index-coded samples was performed on a cBot Cluster Generation System using TruSeq PE Cluster Kit v3-cBotHS (Illumia) following the manufacturer's instructions. The library preparations were sequenced on an Illumina Hiseq platform and 150 bp paired-end reads were generated after cluster generation. Raw data (raw reads) in fastq format were firstly processed through in-house Perl scripts. Clean data (clean reads) were obtained by removing reads containing adapters, and the reads mainly included low-quality reads and ploy-N from raw data. We directly downloaded the reference genome and gene model annotation files from the genome website. The index of the reference genome was built by using STAR and paired-end clean reads were aligned to the reference genome using STAR (v2.5.1b). The method of Maximal Mappable Prefix (MMP) was used in STAR. HTSeq v0.6.0 was used to count the read numbers mapped to each gene. Analysis of differential expression was performed using the edgeR R package (3.12.1). The *P* values were adjusted by using the Benjamini and Hochberg method.

Echocardiography

Echocardiography was performed on the 14th day after CAL using the ultra-high-resolution ultrasound system (Vevo 3100LT, Visual Sonics, Toronto, Canada). Left ventricle posterior wall in diastole (LVPW;d), interventricular septum in diastole (IVS;d), and left ventricle interior diameter in diastole (LVID;d) were measured by M-mode tracing. Left ventricular ejection fraction (LVEF), left ventricular fractional shortening (LVFS), left ventricular volume in diastole (LV Vol;d) and stroke volume (SV) were calculated using Vevo® LAB Software V3.2.6.

Histopathologic examination

The heart tissues of mice were removed on the 14th day after CAL and fixed in 10% phosphate-buffered formalin for 24 h before paraffin embedding. Then, the paraffin sections (4–5 μm in thickness) of the heart were stained by H&E, Masson's trichrome, and Sirius Red staining [34]. The sections were pictured under a light microscope (DX45, Olympus Microsystems Ltd., Japan). The H&E sections were assessed by pathologists without the information of the samples. The collagen volume fraction (CVF) of Masson and Sirius Red staining was quantified using ImageJ program.

Immunohistochemistry

The heart tissues of mice were removed on the 14th day after CAL and fixed in 4% paraformaldehyde. Then the tissues were embedded in paraffin. Hydrated paraffin sections (4–5 μm in thickness) were deparaffinized, rehydrated in phosphate-buffered saline (PBS), and incubated with 3% hydrogen peroxide to block endogenous peroxidase activity. The sections were incubated at 4 °C overnight with anti-collagen type III alpha 1 (COL3A1), anti-collagen-1 (COL1A), or anti-ACY1 primary antibodies after being blocked with blocking liquid. Thereafter, the sections were washed with PBS and incubated with HRP-conjugated secondary antibodies for 1 h at room temperature. Images were acquired using the light microscope (DX45, Olympus Microsystems Ltd., Japan) [35].

Cell culture and treatment

Mice cardiac fibroblasts (MCFs) were obtained from Soochow University and cultured in DME/F-12 medium supplemented with 10% fetal bovine serum, 100 U/mL penicillin, and 100 μg/mL streptomycin at 37 °C in a humidified atmosphere with 5% CO_2. The culture medium was replaced every 2 days. MCFs were subcultured at 80%–90% confluence.

MCFs were cultured for 24 h and then transfected with ACY1-plasmid at 60%–70% confluence. MCFs were transfected with ACY1-plasmid or control (final concentration, 1 μg/mL) for 12 h using 2 μL/mL of Hyper Transfection Plus according to the manufacturer's protocol. Then the culture medium was replaced with fresh DME/F-12 medium supplemented with 10% fetal bovine serum and the cells were cultured for another 36 h.

MCFs were cultured for 24 h and then transfected with ACY1-siRNA at 60%–70% confluence. MCFs were transfected with ACY1-siRNA or control (final concentration, 100 nM) for 6 h using 6 μL/mL Lipofectamine™ 2000 according to the manufacturer's protocol. Then the culture medium was replaced with fresh DME/F-12 medium supplemented with 10% fetal bovine serum, 100 U/mL penicillin, and 100 μg/mL streptomycin and the cells were cultured for another 48 h.

The normal MCFs, ACY1-plasmid-transfected MCFs and ACY1-siRNA-transfected MCFs were stimulated with angiotensin II (Ang II) (1 μM) and treated with different doses of Rg3 for 24 h. Then the cells were subjected to the following experimental procedures.

MTT assay

MCFs were plated at 7×10^5 cells/well (96 well plates) and cultured for 24 h. MCFs were then cultured with fresh medium containing Ang II (1 μM) or Rg3 (1, 5, and 25 μM) for another 24 h, respectively. MTT (0.5 mg/mL) was added to each well for another 4 h incubation at 37 °C to detect the cell viability. After dissolving the crystal with 150 μL dimethyl sulfoxide, the absorbance was measured at 570 nm with a reference wavelength of 650 nm with a microplate reader. The cell viability was expressed as the percentage of absorbance to control values [36].

Immunofluorescence

The heart tissues of mice were removed on the 14th day after CAL. The tissues were snap-frozen and cryosectioned (10 μm in thickness). The slices of the heart were washed with PBS, fixed in 4% paraformaldehyde, and permeabilized with PBS containing 0.1% Triton X-100. The tissues were then blocked at room temperature with 5% bovine serum albumin and incubated with primary antibody overnight at 4 °C. Then the secondary antibody incubation was performed and nuclei were visualized with DAPI.

MCFs were cultured on the glass-bottom dish. The cells were washed with PBS, fixed with ice-cold 4% paraformaldehyde, and permeabilized with PBS containing 0.1% Triton X-100. And the rest of the procedure was conducted as described above. The fluorescence was observed using a confocal laser scanning microscope (CLSM, LSM700, Zeiss, Germany) [37].

Western blotting analysis

The total protein extracted from heart tissues and MCFs was resolved on 12.5% sodium dodecyl sulfate-polyacrylamide gels

and transferred to polyvinylidene difluoride membranes. The membranes were blocked with 5% bovine serum albumin, incubated with primary antibodies overnight at 4 °C, and incubated with the appropriate secondary antibodies at room temperature. The protein signal was detected with the ECL-plus detection system. The band densities were visualized by ChemiDoc™ MP System (Bio-Rad), and the relative values were expressed relative to the signal of GAPDH [38].

Statistical analysis

All values were expressed as mean ± standard deviation. Student's *t* test, Mann–Whitney test, and one-way analysis of variance were performed to determine the statistical significance among values. *P* values < 0.05 and 0.01 were regarded as significant and very significant, respectively. The SPSS 19.0 statistical analysis software was used for the statistical analysis.

RESULTS

Metabolite *N*-acetylglutamine was elevated and the expression of ACY1 was decreased in patients with HF and CAL-induced HF mice

The levels of urinary *N*-acetylglutamine were significantly elevated in both HF patients (Fig. 1a) and CAL-induced HF mice (Fig. 1b). Based on these findings, transcriptomics was adopted to excavate the key regulatory enzyme that caused the abnormal increase of *N*-acetylglutamine in HF. The gene expression of its specific degradation enzyme ACY1 was found to be significantly decreased in the heart tissue of HF mice (Fig. 1c). Western blotting and immunohistochemical techniques were further performed to verify that the protein expression of ACY1 in heart tissue of HF mice was significantly decreased (Fig. 1d, e), which suggested that ACY1 may play a role in the development of HF.

Inhibition of ACY1 aggravated the formation of myocardial fibrosis and activated the pathway of TGF-β1/Smad3 in HF mice

To elucidate the function of ACY1 in HF, the sham and HF model group mice were injected intraperitoneally with the inhibitor of ACY1 (MTBM), which could effectively decrease the expression of ACY1 in the heart tissue of sham and HF mice (Supplementary Figure S2). Then the cardiac function, myocardial pathology, and collagen expression were examined. As shown in Fig. 2a, LVEF, LVFS, and SV in the model group were significantly diminished, while LVPW;d, LVID;d, IVS;d, and LV Vol;d in the model group were significantly increased compared to the sham group. Furthermore, the sham and HF mice treated with MTBM exhibited worse cardiac function in all the above indexes, which illustrated that ACY1 inhibition exacerbated cardiac dysfunction in HF mice. Haematoxylin–eosin (H&E), Masson's trichrome, and Sirius Red staining results further showed that the heart tissues in the model group had the obvious inflammatory cell infiltration, irregularly arranged cardiomyocytes, swelling of cardiomyocytes, and collagen deposition compared with the sham group (Fig. 2b, Supplementary Figure S3a–c). And MTBM significantly exacerbated the pathological damage and myocardial fibrosis in both sham and model mice. In addition, the expression of COL3A1, COL1A, TGF-β1,

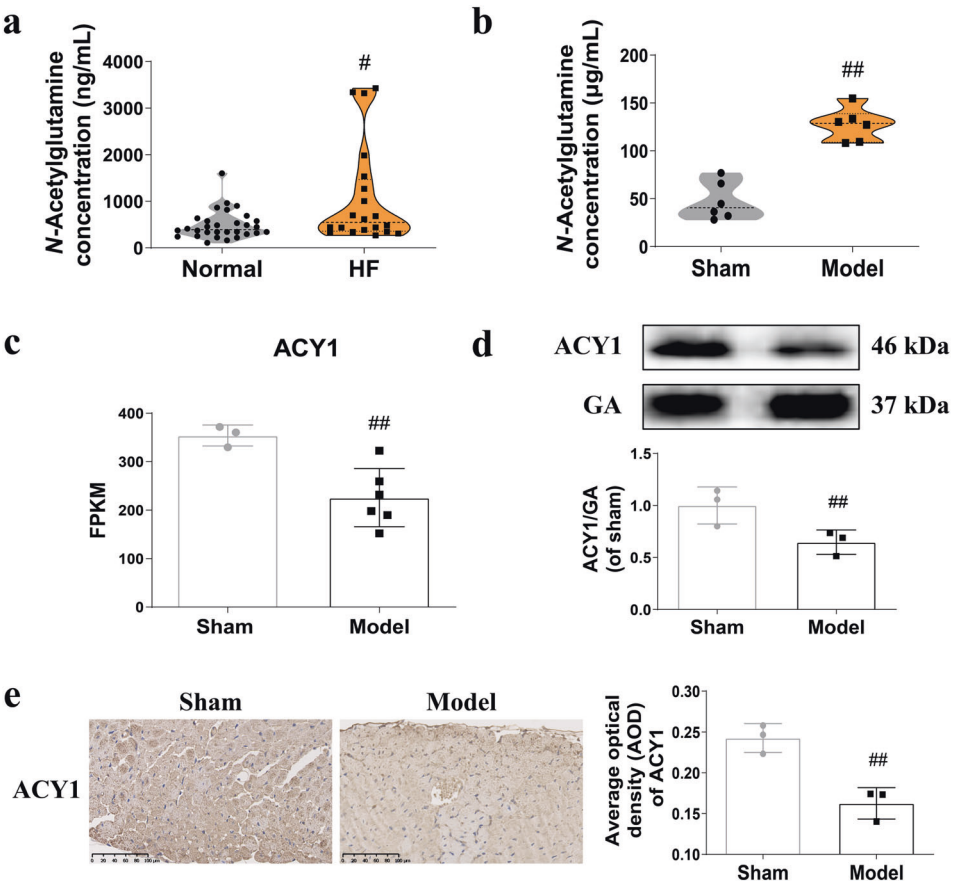

Fig. 1 Metabolite *N*-acetylglutamine was elevated and the expression of ACY1 was decreased in patients with HF and CAL-induced HF mice. a The content of *N*-acetylglutamine in urine samples from humans ($n = 20$–30). **b** The content of *N*-acetylglutamine in urine samples from mice ($n = 6$). **c** The RNA level of ACY1 in heart tissues of HF mice after 2 weeks' CAL based on transcriptome results (Sham: $n = 3$, Model 2–3 week: $n = 6$). **d** Western blotting determined the expression of ACY1 in heart tissues from mice ($n = 3$). **e** Immunohistochemistry determined the expression of ACY1 in heart tissues from mice ($n = 3$). $^{\#}P < 0.05$ vs. Normal group, $^{\#\#}P < 0.01$ vs. Sham group.

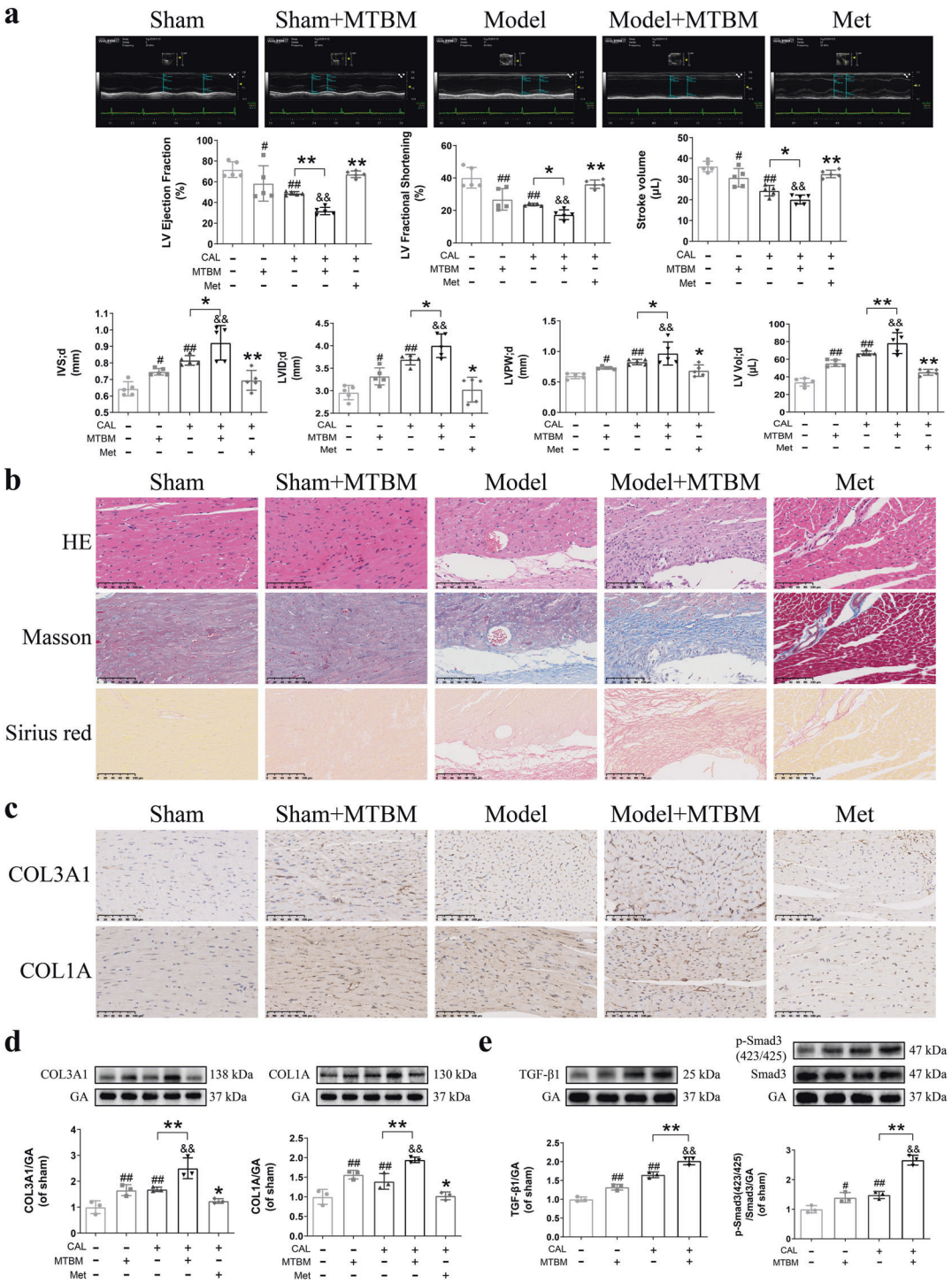

Fig. 2 Inhibition of ACY1 aggravated the formation of myocardial fibrosis and activated the pathway of TGF-β1/Smad3 in HF mice. **a** Representative echocardiographs and the changes of cardiac functions and dimensions in different groups of mice. Cardiac function and dimensions evaluation indexes mainly include LVEF, LVFS, SV, LVPW;d, LVID;d, IVS;d and LV Vol;d ($n = 5$). **b** The pathological changes were determined by H&E staining. The myocardial fibrosis levels were determined by Masson and Sirius red staining ($n = 3$) (×200 magnification). **c** The expression of collagen III and collagen I in the heart tissues of each group of mice was measured by immunohistochemical staining ($n = 3$) (×400 magnification). **d** The expression of collagen III and collagen I in the heart tissues of each group of mice was determined by Western blotting ($n = 3$). **e** The expression of TGF-β1, p-Smad3, and Smad3 in the heart tissues of each group of mice was determined by Western blotting ($n = 3$). $^{\#}P < 0.05$ vs. Sham group, $^{\#\#}P < 0.01$ vs. Sham group, $^{*}P < 0.05$ vs. Model group, $^{**}P < 0.01$ vs. Model group, $^{\&\&}P < 0.01$ vs. Sham+MTBM group.

and p-Smad3/Smad3 were found to be significantly increased in the model group (Fig. 2c–e, Supplementary Figure S3d, e), and the collagen levels and TGF-β1/Smad3 signaling pathway of normal mice and HF mice were markedly elevated by ACY1 inhibitor MTBM. All these results suggested that ACY1 inhibition could result in myocardial structural and functional impairment via the exacerbation of fibrosis through the activation of the TGF-β1/Smad3 signaling pathway.

ACY1 regulated collagen expression and TGF-β1/Smad3 signaling pathway in Ang II-treated MCFs

To further explore the key role of ACY1 in myocardial fibrosis, ACY1-plasmid or ACY1-siRNA were adopted to investigate its regulation on the expression of collagen III, collagen I, and TGF-β1/Smad3 signaling pathway in MCFs treated with Ang II. Western blotting was conducted to verify the success of both ACY1 overexpression or silencing and the results were shown in Supplementary Figure S4. And it was also proved that Ang II could significantly increase the expression of COL3A1, COL1A, and TGF-β1/Smad3 signaling pathways in MCFs treated with control-plasmid or control-siRNA (Fig. 3). Importantly, the expression of COL3A1, COL1A, and TGF-β1/Smad3 signaling pathway in MCFs treated with ACY1-plasmid and Ang II significantly decreased compared with those in MCFs treated with control-plasmid and Ang II, which suggested that overexpression of ACY1 significantly suppressed Ang II-induced collagen expression and TGF-β1/Smad3 signaling pathway in MCFs (Fig. 3a, b). Meanwhile, there were no significant differences between the MCFs treated with control-plasmid and the MCFs treated with ACY1-plasmid in the parameters above. In addition, treatment with ACY1-siRNA significantly promoted the expression of COL3A1, COL1A and activated TGF-β1/Smad3 signaling pathway in MCFs treated with or without Ang II, which suggested that ACY1 deficiency significantly increased Ang II-induced collagen expression in MCFs via the TGF-β1/Smad3 signaling pathway (Fig. 3c, d). All of the above results revealed that ACY1 has a critical role in myocardial fibrosis via the regulation of TGF-β1/Smad3.

Rg3 decreased the content of *N*-acetylglutamine, increased the expression of ACY1, and inhibited TGF-β1/Smad3 signaling pathway in CAL-induced HF mice and Ang II-treated MCFs

As shown in Fig. 4a, 20(*S*)-ginsenoside Rg3 significantly reduced CAL-induced elevation of *N*-acetylglutamine in HF mice, which suggested that both ACY1 and ACY1-mediated TGF-β1/Smad3 signaling pathway demonstrated above might be regulated by Rg3. As illustrated in Fig. 4b–f, compared with the model group, Rg3 significantly increased the expression of ACY1 which hydrolyzes *N*-acetylglutamine, and inhibited the expression of TGF-β1/Smad3, which stimulates myocardial fibrosis in vivo and in vitro. The above results implied that Rg3 has the potential to improve HF via the regulation of myocardial fibrosis.

Rg3 ameliorated cardiac function and myocardial fibrosis in CAL-induced HF mice and Ang II-induced MCFs

The effect of Rg3 on cardiac function of HF mice was evaluated with echocardiography (Fig. 5a). The results showed that LVEF, LVFS, and SV of HF mice were significantly improved by Rg3 and Met, while LVPW;d, LVID;d, IVS;d, and LV Vol;d of HF mice were significantly reduced by Rg3 and Met, and the effect of Rg3 with the high dosage on HF was comparable with that of Met. H&E, Masson's trichrome, and Sirius Red staining were further performed to evaluate the improvement of Rg3 on cardiac pathology and myocardial fibrosis. The results showed that treatment with Rg3 or Met significantly alleviated the degree of morphological damages and myocardial fibrosis in HF mice (Fig. 5b, Supplementary Figure S5a–c). The effect of Rg3 on collagen deposition in CAL-induced HF mice and Ang II-induced MCFs was also detected. The immunohistochemical analysis disclosed that Rg3 significantly reduced the expression of COL3A1 and COL1A in heart tissues of HF mice (Fig. 5c, Supplementary Figure S5d, e). Moreover, Western blotting results showed that the levels of COL3A1, COL1A, α-smooth muscle actin (α-SMA), and tissue inhibitor of metalloproteinase-1 (TIMP-1)/matrix metalloproteinase-1 (MMP-1) ratio associated with myocardial fibrosis were significantly upregulated in CAL-induced HF mice, while the indices above were significantly reduced by Rg3 (Fig. 5d). Meanwhile, these findings were further verified in Ang II-induced MCFs. The results of cell viability proved that 20(*S*)-ginsenoside Rg3 (1, 5, and 25 μM) exhibited no cytotoxicity against MCFs (Supplementary Figure S6), and the inhibitory effect on myocardial fibrosis-associated proteins was basically consistent with the results in vivo (Fig. 5e). All these results suggested that Rg3 could prevent myocardial fibrosis to improve HF.

ACY1 exerted an important role in Rg3 inhibiting myocardial fibrosis and TGF-β1/Smad3 signaling pathway in Ang II-treated MCFs

ACY1-plasmid and ACY1-siRNA were applied to further confirm the specific role of ACY1 in the regulation of myocardial fibrosis and TGF-β1/Smad3 signaling pathway by Rg3. As shown in Fig. 6a and b, the intervention of ACY1-plasmid further promoted the inhibitory effect of Rg3 on collagen and TGF-β1/Smad3 expression in MCFs treated with Ang II, which means that overexpression of ACY1 will slightly facilitate the ameliorative effect of Rg3 on myocardial fibrosis. More importantly, Fig. 6c and d also indicated that ACY1-siRNA significantly weakened the effect of Rg3 in inhibiting collagen I deposition and TGF-β1/Smad3 pathway in Ang II-induced MCFs. All these results suggested that ACY1 might be the key functional protein for Rg3 to inhibit myocardial fibrosis and the TGF-β1/Smad3 pathway.

DISCUSSION

In recent years, particular attention is paid to the role of metabolism in many diseases and metabolites could provide insight into the pathological mechanisms of complex diseases. Our previous research has shown that there was a significant difference in the content of metabolite *N*-acetylglutamine between CAL-induced HF mice and the normal mice (Supplementary Table S3), but further targeted verification is still needed. This study firstly proved that the levels of *N*-acetylglutamine in HF patients and CAL-induced HF mice both significantly increased through targeted metabolomic analysis using HPLC-QqQ-MS, which suggested that *N*-acetylglutamine may be the potential biomarker of HF. *N*-acetylglutamine is a metabolite present in the urine of healthy people and markedly increases when organ damage or tumors occurs [39, 40]. Meanwhile, ACY1 is the specific metabolic-degrading enzyme of *N*-acetylglutamine, and is closely associated with its abnormal elevation [41]. Therefore, the change of ACY1 expression in heart tissue of HF mice was further investigated. And the results showed that the expression of ACY1 was significantly decreased in HF mice, which was consistent with the transcriptomic results. All these findings confirmed that the abnormal elevation of *N*-acetylglutamine in HF was closely related to the inhibition of ACY1, and also suggested that ACY1 might play a critical role in the development of HF.

ACY1 is a cytosolic enzyme that deacylates the α-acylated amino acid from the N-terminal peptide of intracellular proteins [42]. Previous studies have shown that ACY1 is important for regulating the proliferation of numerous types of cancer [43], sunch as colonic cancer [44], hepatocellular carcinoma [45], and renal cell carcinoma [46]. However, the function of ACY1 in HF and myocardial fibrosis remains unclear. To explore the specific role of ACY1 in HF, the inhibitor of ACY1 (MTBM) was adopted to investigate the effect on cardiac function and pathology. Cardiac function and dimensions indexes mainly include LVEF, LVFS, SV, LVPW;d, LVID;d, IVS;d, and LV Vol;d. Therein, LVEF, LVFS, and SV are commonly applied in clinical practice to evaluate the ejection ability of the left ventricle, the amplitude of ventricular contraction, and the force of ventricular contraction, respectively [47]. LVPW;d, LVID;d, IVS;d, and LV Vol;d is used to measure the cardiac wall thickness and volumes to evaluate the cardiac remodeling, which is associated with worsening cardiac function and poor prognosis [48]. The parameters above were all aggravated by ACY1 inhibitor and the results suggested that ACY1 inhibition

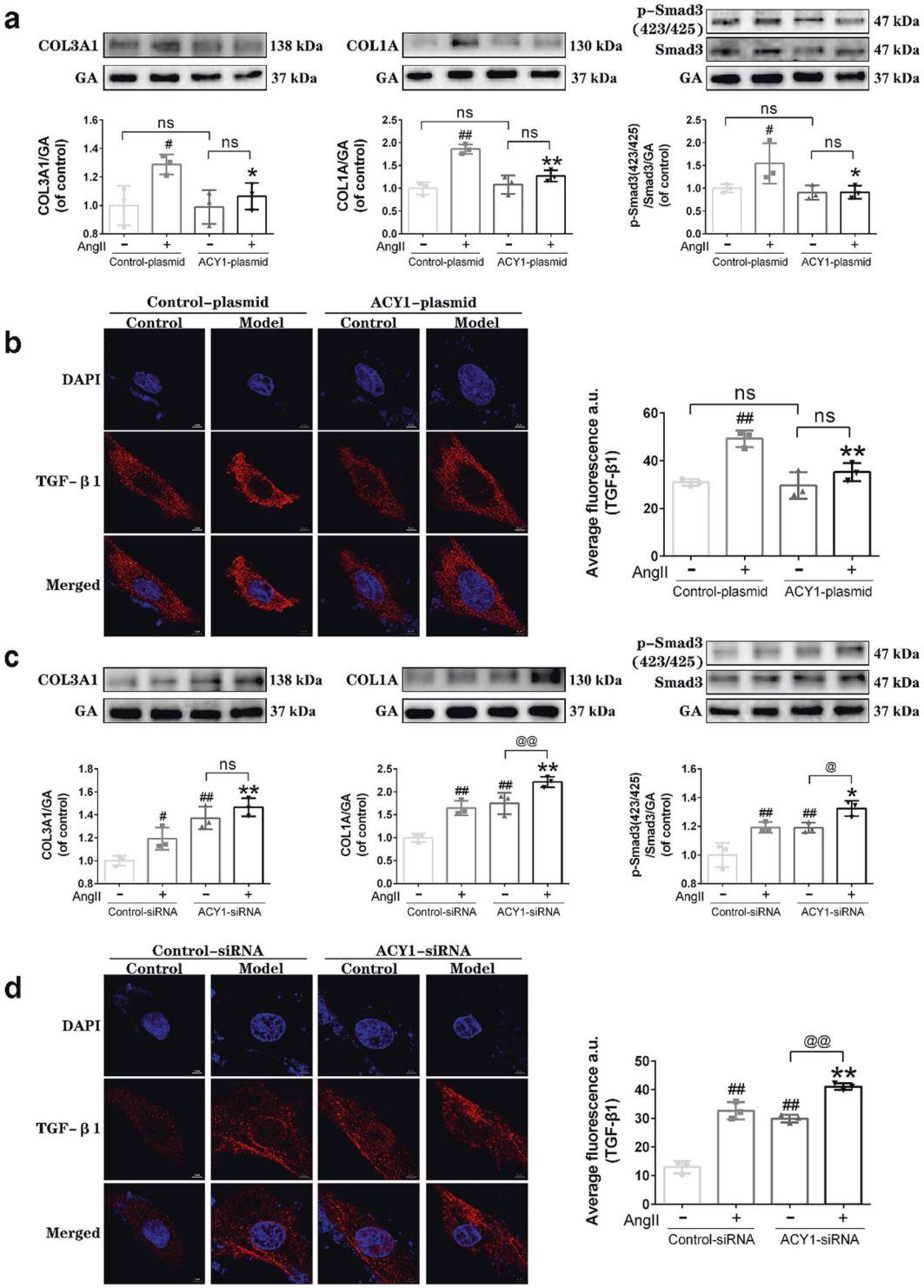

Fig. 3 ACY1 regulated collagen expression and TGF-β1/Smad3 signaling pathway in Ang II-treated MCFs. a The expression of collagen III, collagen I, p-Smad3, and Smad3 were determined by Western blotting in Ang II-induced MCFs treated with ACY1-plasmid or control-plasmid ($n = 3$). **b** Representative immunofluorescence analysis of TGF-β1 in Ang II-induced MCFs treated with ACY1-plasmid or control-plasmid ($n = 3$). **c** The expression of collagen III, collagen I, p-Smad3, and Smad3 were determined by Western blotting in Ang II-induced MCFs treated with ACY1-siRNA or control-siRNA ($n = 3$). **d** Representative immunofluorescence analysis of TGF-β1 in Ang II-induced MCFs treated with ACY1-siRNA or control-siRNA ($n = 3$). $^{\#}P < 0.05$ vs. Control group without Ang II, $^{\#\#}P < 0.01$ vs. Control group without Ang II, $^{*}P < 0.05$ vs. group treated with Ang II alone, $^{**}P < 0.01$ vs. group treated with Ang II alone, $^{@}P < 0.05$ vs. group treated with ACY1-siRNA alone, $^{@@}P < 0.01$ vs. group treated with ACY1-siRNA alone.

could further exacerbate cardiac pumping dysfunction and structural abnormalities in HF mice. In addition, pathological results of heart tissues showed that ACY1 inhibition resulted in significant myocardial fibrosis in normal mice and also obviously exacerbated the myocardial fibrosis in HF mice, which indicated that ACY1 might exert a prominent role in myocardial fibrosis.

Myocardial fibrosis is pathologically characterized by increased deposition of collagen III and collagen I, which causes increased

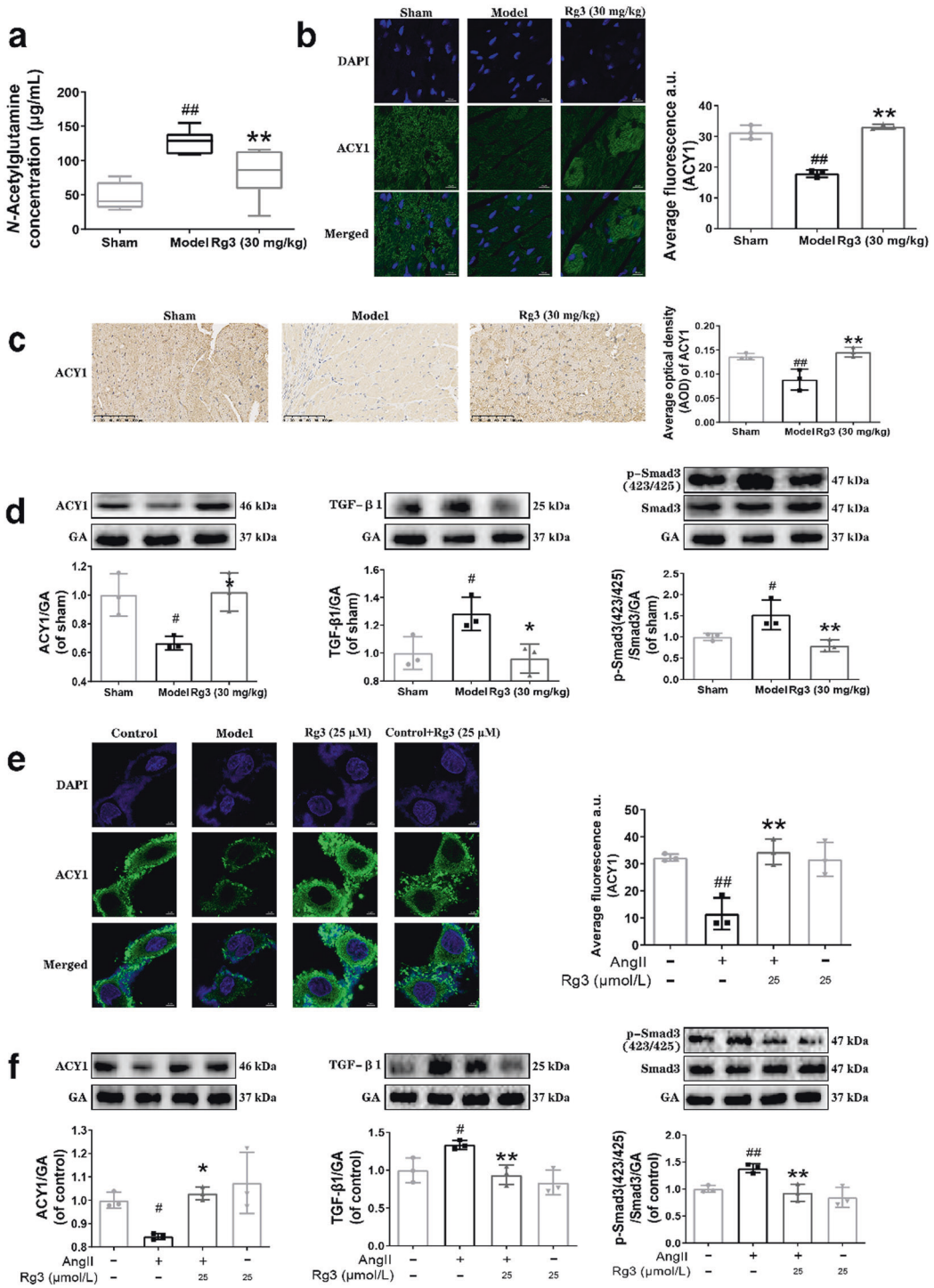

Fig. 4 Rg3 decreased the content of *N*-acetylglutamine, increased the expression of ACY1, and inhibited TGF-β1/Smad3 signaling pathway in CAL-induced HF mice and Ang II-treated MCFs. a The content of *N*-acetylglutamine in urine samples of each group mice was determined by LC–MS ($n = 6$). **b** The expression of ACY1 in heart tissues of each group of mice was determined by immunofluorescence ($n = 3$). **c** The expression of ACY1 in heart tissues of each group of mice was determined by immunohistochemistry ($n = 3$). **d** Representative Western blotting analysis of the expression of ACY1, TGF-β1, p-Smad3, and Smad3 in heart tissues of each group mice ($n = 3$). **e** Representative immunofluorescence analysis of the expression of ACY1 in Ang II-induced MCFs ($n = 3$). **f** Representative Western blotting analysis of the expression of ACY1, TGF-β1, p-Smad3, and Smad3 in Ang II-induced MCFs ($n = 3$). $^{\#}P < 0.05$ vs. Sham group or Control group, $^{\#\#}P < 0.01$ vs. Sham group or Control group, $^{*}P < 0.05$ vs. Model group or group treated with Ang II alone, $^{**}P < 0.01$ vs. Model group or group treated with Ang II alone.

matrix stiffness and abnormal cardiac function, leading to HF [49]. Collagen III (12%) and collagen I (70%) are the major fibrillar components in the heart [50]. And collagen I is a relatively stiff protein that determines tissue stiffness, hence considered as the key player for controlling the development of myocardial fibrosis [51]. And most studies have focused on the evaluation of collagen I to explore the effects of specific factors on myocardial fibrosis [52–54]. In addition, activation of TGF-β1/Smad3 is also a classical

signaling pathway of myocardial fibrosis [8]. Thus, the effect of ACY1 inhibition on collagen III and collagen I, and the TGF-β1/Smad3 signaling pathway were further explored. The results showed that the expression of collagens and TGF-β1 stimulation of Smad3 phosphorylation in both normal mice and HF mice were significantly increased by the inhibition of ACY1, which inferred that ACY1 inhibition could aggravate HF via the exacerbation of fibrosis through the TGF-β1/Smad3 signaling pathway.

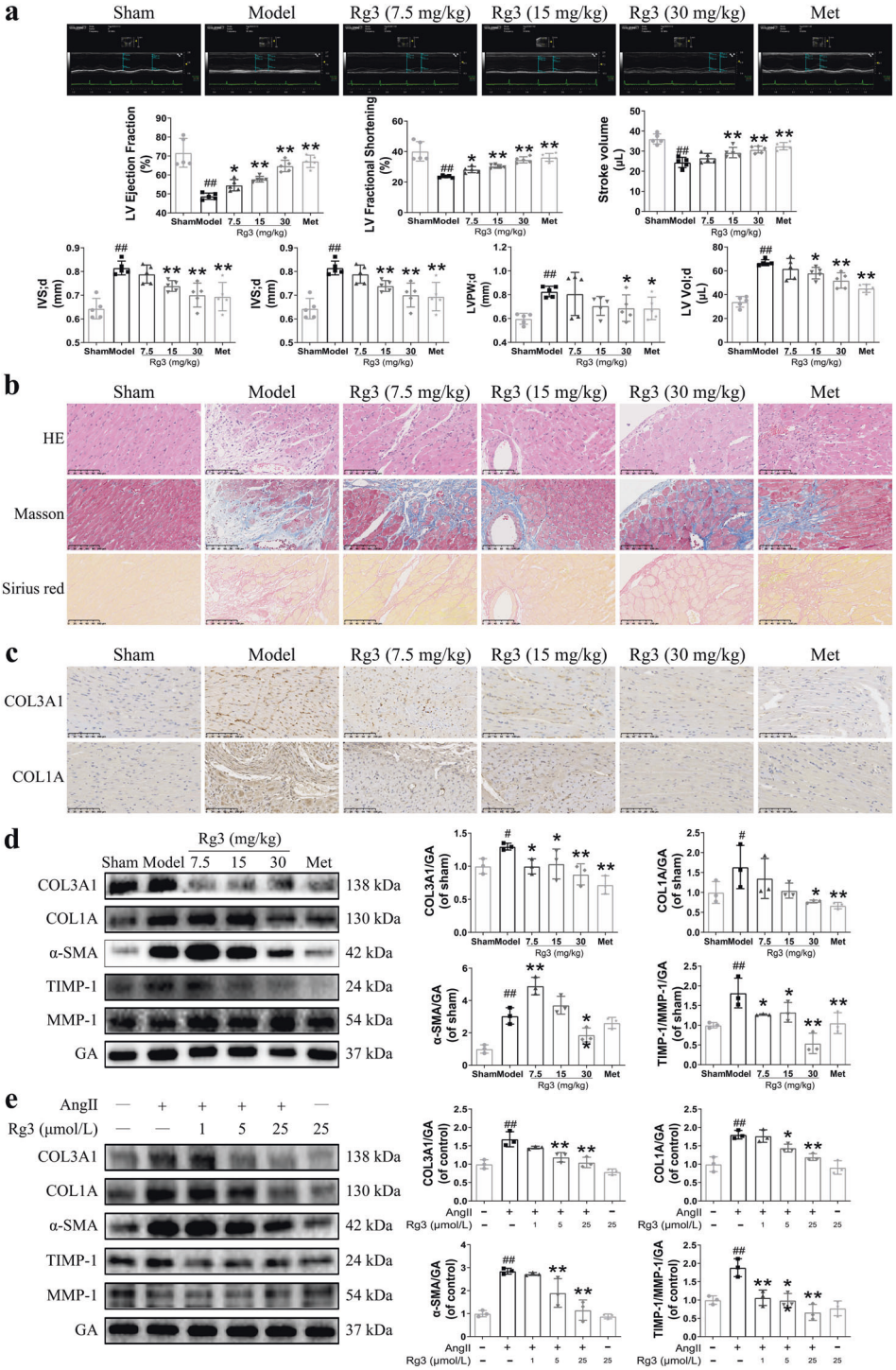

Fig. 5 Rg3 ameliorated cardiac function and myocardial fibrosis in CAL-induced HF mice and Ang II-induced MCFs. a Representative echocardiographs and the changes of cardiac functions and dimensions in different groups of mice. Cardiac function and dimensions evaluation indexes mainly include LVEF, LVFS, SV, LVPW;d, LVID;d, IVS;d, and LV Vol;d ($n = 5$). **b** The pathological changes were determined by H&E staining. The myocardial fibrosis levels were determined by Masson and Sirius red staining ($n = 3$) (×200 magnification). **c** The expression of collagen III and collagen I in the heart tissues of each group was measured by immunohistochemical staining ($n = 3$) (×400 magnification). **d** Representative Western blotting analysis of the expression of collagen III, collagen I, α-SMA, TIMP-1, and MMP-1 in heart tissues ($n = 3$). **e** Representative Western blotting analysis of the expression of collagen III, collagen I, α-SMA, TIMP-1, and MMP-1 in Ang II-induced MCFs ($n = 3$). $^{\#}P < 0.05$ vs. Sham group, $^{\#\#}P < 0.01$ vs. Sham group or Control group, $^{*}P < 0.05$ vs. Model group or group treated with Ang II alone, $^{**}P < 0.01$ vs. Model group or group treated with Ang II alone.

Cardiac fibroblasts undergo conversion to myofibroblasts in infarcted hearts, which is the crucial cellular event in myocardial fibrosis [55]. In this study, MCFs were treated with Ang II to further explore the effect and mechanism of ACY1 on myocardial fibrosis in vitro. Overexpression and knockdown of ACY1 using ACY1-plasmid and ACY1-siRNA in MCFs were performed. The results showed that Ang II-induced collagen III and collagen I deposition as well as TGF-β1/Smad3 pathway expression in MCFs were

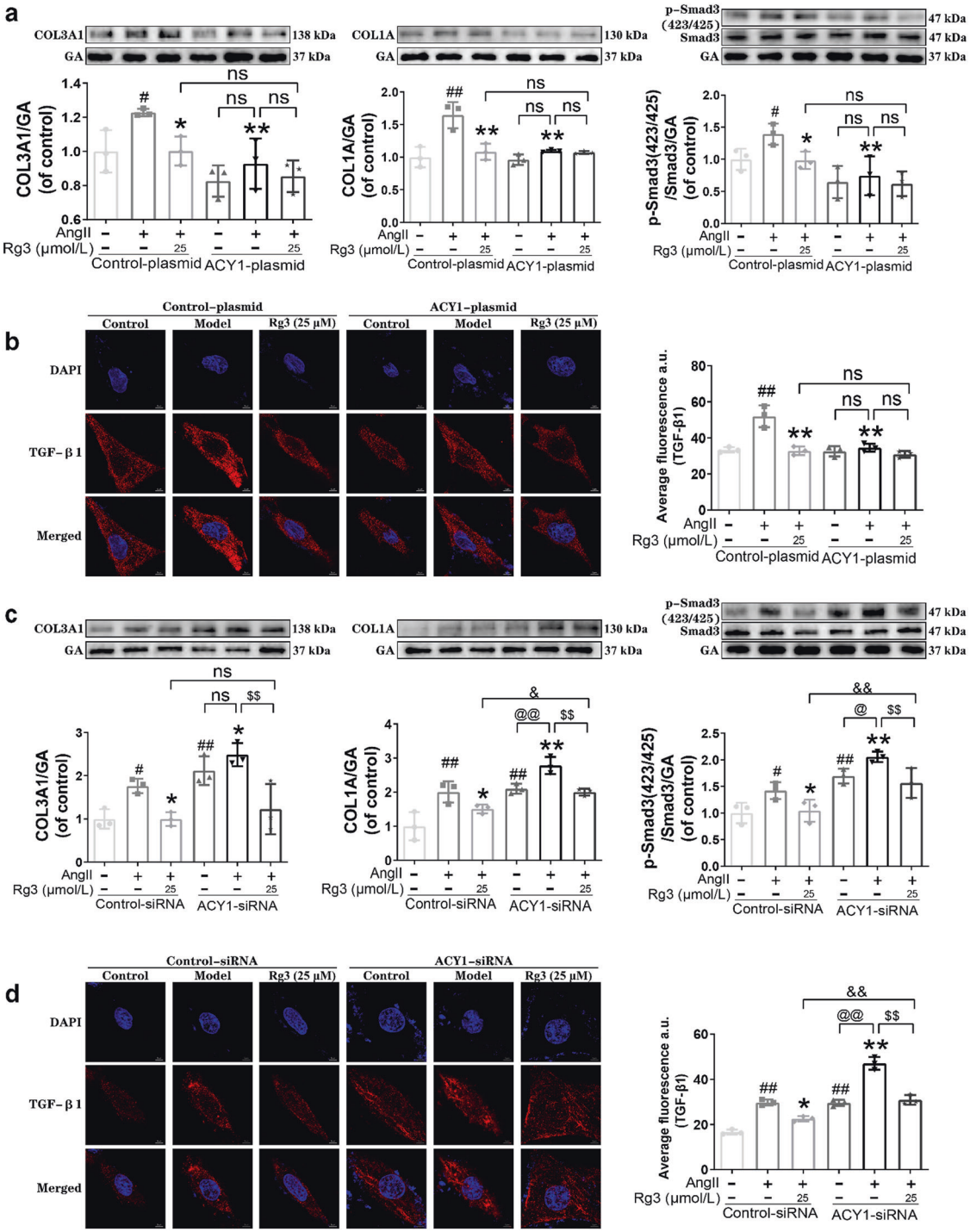

Fig. 6 ACY1 exerted an important role in Rg3 inhibiting myocardial fibrosis and TGF-β1/Smad3 signaling pathway in Ang II-treated MCFs. a Representative Western blotting analysis of the expression of collagen III, collagen I, p-Smad3, and Smad3 in Ang II-induced MCFs treated with ACY1-plasmid, control-plasmid or Rg3 ($n = 3$). **b** Representative immunofluorescence analysis of the expression of TGF-β1 in Ang II-induced MCFs treated with ACY1-plasmid, control-plasmid, or Rg3 ($n = 3$). **c** Representative Western blotting analysis of the expression of collagen III, collagen I, p-Smad3, and Smad3 in Ang II-induced MCFs treated with ACY1-siRNA, control-siRNA, or Rg3 ($n = 3$). **d** Representative immunofluorescence analysis of the expression of TGF-β1 in Ang II-induced MCFs treated with ACY1-siRNA, control-siRNA, or Rg3 ($n = 3$). $^{\#}P < 0.05$ vs. Control group, $^{\#\#}P < 0.01$ vs. Control group, $^{*}P < 0.05$ vs. group treated with Ang II alone, $^{**}P < 0.01$ vs. group treated with Ang II alone, $^{@}P < 0.05$ vs. group treated with ACY1-siRNA alone, $^{@@}P < 0.01$ vs. group treated with ACY1-siRNA alone, $^{\$\$}P < 0.01$ vs. group treated with ACY1-siRNA and Ang II, $^{\&}P < 0.05$ vs. group treated with Rg3 and Ang II, $^{\&\&}P < 0.01$ vs. group treated with Rg3 and Ang II.

significantly inhibited by overexpression of ACY1. Whereas, ACY1 siRNA could facilitate the collagen III and collagen I expression as well as activate the pathway of TGF-β1/Smad3 in MCFs treated with or without Ang II. All of the above findings provided further evidence that ACY1 inhibition is an essential factor in activating the TGF-β1/Smad3 signal pathway and leading to myocardial fibrosis in HF. What's more, it has been reported that ACY1 also plays an important role in cancers and new findings suggest that HF could also be considered as interstitial cancer [45, 56, 57]. Therefore, regulation of ACY1 might be the potential approach to ameliorate myocardial fibrosis to improve HF as well.

Panax ginseng C.A. Meyer (Araliaceae) is the most widely used TCM in the treatment of HF and ginsenoside Rg3 is one of the active components isolated from it. It has been reported that ginsenoside Rg3 had protective effects on many cardiovascular diseases [58], while the effects and mechanisms of Rg3 on HF still need further study. In the present study, we firstly found that 20(*S*)-ginsenoside Rg3 could decrease the levels of *N*-acetylglutamine in HF mice, increase the expression of ACY1 in HF mice and Ang II-induced MCFs, and also inhibit the TGF-β1/Smad3 pathway in vivo and in vitro, which suggested that ginsenoside Rg3 might have a therapeutic effect on HF via the regulation of myocardial fibrosis.

Subsequently, we further explored the effect of 20(*S*)-ginsenoside Rg3 on cardiac function and dimensions, pathology, and collagen expression in HF mice. The results of echocardiography showed that ginsenoside Rg3 obviously improved myocardial contractility, pumping ability, and pathological ventricular remodeling in HF mice. And the pathological results also indicated that ginsenoside Rg3 could significantly improve myocardial fibrosis in HF mice. It is widely accepted that α-SMA is the characteristic marker of cardiac fibroblast differentiation, which is the key event in the production of collagens in myocardial fibrosis [59]. And the increased collagen deposition in HF is regarded as the imbalance between collagen synthesis and its degradation [60]. The insoluble collagen fibers would be degraded by MMP-1, which is inhibited by TIMP-1. And the collagen deposition would be reduced when MMP-1 is increased or TIMP-1 is decreased [60]. Therefore, the expression of collagen III, collagen I, α-SMA, TIMP-1, and MMP-1 associated with myocardial fibrosis was further detected in HF mice and Ang II-induced MCFs. The results illustrated that 20(*S*)-ginsenoside Rg3 could maintain collagen metabolism balance via inhibition of collagen synthesis and facilitation of collagen degradation to attenuate myocardial fibrosis in HF mice and Ang II-induced MCFs.

Additionally, whether ACY1 plays an important role in the cardioprotection of 20(*S*)-ginsenoside Rg3 was also elucidated. ACY1-plasmid and ACY1-siRNA were further performed to explore the effect of ACY1 on the inhibitory effect of ginsenoside Rg3 on collagen expression and TGF-β1/Smad3 pathway activation in Ang II-treated MCFs. The results exhibited that overexpression of ACY1 slightly facilitated the inhibitory effect of ginsenoside Rg3 on collagen expression and TGF-β1/Smad3 activation. Conversely, ACY1 siRNA partially weakened the beneficial effects of ginsenoside Rg3. These evidences further confirmed that ACY1 is essential or even a key functional protein for Rg3 to exert an inhibitory effect on myocardial fibrosis. And it also revealed that ginsenoside Rg3 could indirectly inhibit TGF-β1/Smad3 pathway via the regulation of ACY1, which provided a reference for the development of anti-myocardial fibrosis medicine to avoid the side effects caused by the direct inhibition of TGF-β1/Smad3 [9]. However, potential limitations of this study should be noted. Although the present study investigated the effects of Rg3 on myocardial fibrosis with ACY1 siRNA or overexpression, further study needs to validate ACY1 knock-out or knock-in mice in the future.

In summary, this study demonstrated that metabolite *N*-acetylglutamine is abnormally elevated in HF and might be the potential biomarker of HF, which provided a reference for the diagnosis of HF in the future. And its specific metabolic-degrading enzyme ACY1 expression is significantly decreased and is closely associated with myocardial fibrosis in HF. Overexpression of ACY1 could effectively inhibit the deposition of collagen and the activation of TGF-β1/Smad3 pathway, which indicated that it could be a potential therapeutic target for the prevention and treatment of myocardial fibrosis during the development of HF. More interestingly, 20(*S*)-ginsenoside Rg3 has been found to ameliorate myocardial fibrosis to improve HF through the ACY1-mediated TGF-β1/Smad3 pathway, which not only enriched the clinical application of 20(*S*)-ginsenoside Rg3 in HF, but also provided some references for the further development of anti-fibrotic medicine for HF (Fig. 7).

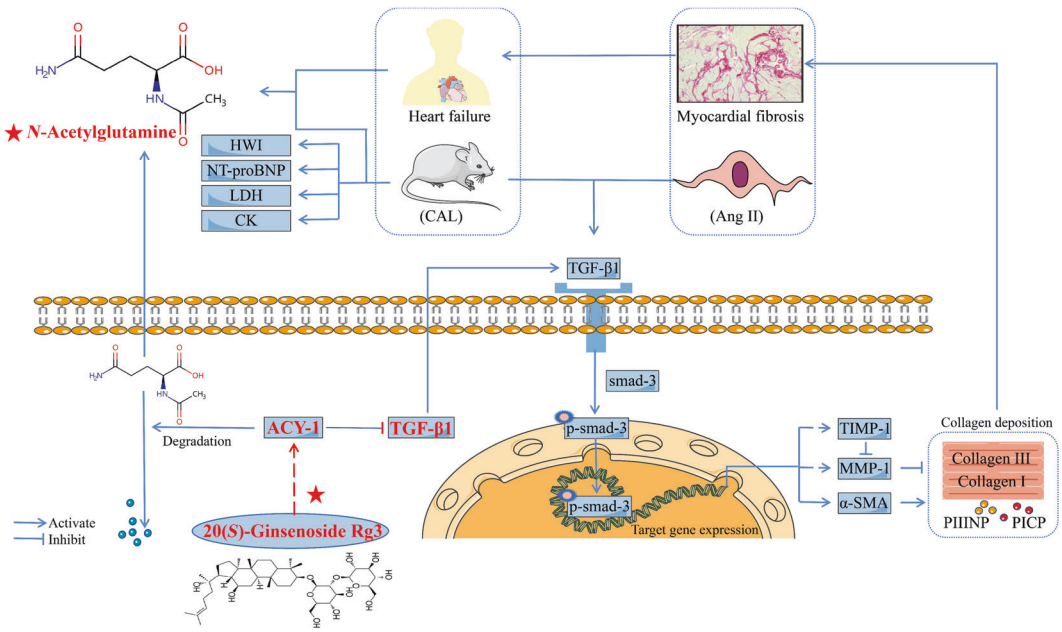

Fig. 7 The key role of aminoacylase-1 in myocardial fibrosis and the regulatory effect of 20(*S*)-ginsenoside Rg3 in heart failure. *N*-acetylglutamine is abnormally elevated in HF and may be the potential biomarker of HF. And its specific metabolic-degrading enzyme ACY1 expression is significantly decreased and has played a critical role in myocardial fibrosis during the development of HF. Rg3 could ameliorate myocardial fibrosis to improve HF through ACY1-mediated TGF-β1/Smad3 pathway.

ACKNOWLEDGEMENTS

This research work was supported by the National Natural Science Foundation of China (81774150, 81973506, 82104437), Natural Science Foundation of Jiangsu Province (BK20210431), China Postdoctoral Science Foundation (2021M693519), National Innovation and Entrepreneurship Training Program for Undergraduate (202110316013Y) and "Double First-Class" University project (CPU2018GF06, CPU2018GF07).

AUTHOR CONTRIBUTIONS

BYY and FL designed research; QL, FML, and WLR performed research; GYY, ZYF, and LZ contributed new reagents or analytic tools; FF and JPK analyzed data; FL and QL wrote the paper. All the authors have approved the manuscript.

ADDITIONAL INFORMATION

Supplementary information The online version contains supplementary material available at https://doi.org/10.1038/s41401-021-00830-1.

Competing interests: The authors declare no competing interests.

REFERENCES

1. Serenelli M, Jackson A, Dewan P, Jhund PS, Petrie MC, Rossignol P, et al. Mineralocorticoid receptor antagonists, blood pressure, and outcomes in heart failure with reduced ejection fraction. JACC Heart Fail. 2020;8:188–98.
2. González A, Schelbert EB, Díez J, Butler J. Myocardial interstitial fibrosis in heart failure: biological and translational perspectives. J Am Coll Cardiol. 2018;71:1696–706.
3. Truby LK, Rogers JG. Advanced heart failure: epidemiology, diagnosis, and therapeutic approaches. JACC Heart Fail. 2020;8:523–36.
4. Wintrich J, Kindermann I, Ukena C, Selejan S, Werner C, Maack C, et al. Therapeutic approaches in heart failure with preserved ejection fraction: past, present, and future. Clin Res Cardiol. 2020;109:1079–98.
5. Heymans S, González A, Pizard A, Papageorgiou AP, López-Andrés N, Jaisser F, et al. Searching for new mechanisms of myocardial fibrosis with diagnostic and/or therapeutic potential. Eur J Heart Fail. 2015;17:764–71.
6. Gyöngyösi M, Winkler J, Ramos I, Do QT, Firat H, McDonald K, et al. Myocardial fibrosis: biomedical research from bench to bedside. Eur J Heart Fail. 2017;19:177–91.
7. Guo Y, Gupte M, Umbarkar P, Singh AP, Sui JY, Force T, et al. Entanglement of GSK-3β, β-catenin and TGF-β1 signaling network to regulate myocardial fibrosis. J Mol Cell Cardiol. 2017;110:109–20.
8. Rodriguez P, Sassi Y, Troncone L, Benard L, Ishikawa K, Gordon RE, et al. Deletion of delta-like 1 homologue accelerates fibroblast-myofibroblast differentiation and induces myocardial fibrosis. Eur Heart J. 2019;40:967–78.
9. Zhao X, Kwan JYY, Yip K, Liu PP, Liu FF. Targeting metabolic dysregulation for fibrosis therapy. Nat Rev Drug Discov. 2020;19:57–75.
10. Tallquist MD. Cardiac fibroblast diversity. Annu Rev Physiol. 2020;82:63–78.
11. Bajaj JS, Reddy KR, O'Leary JG, Vargas HE, Lai JC, Kamath PS, et al. Serum levels of metabolites produced by intestinal microbes and lipid moieties independently associated with acute-on-chronic liver failure and death in patients with cirrhosis. Gastroenterology. 2020;159:1715–30.
12. Figlia G, Willnow P, Teleman AA. Metabolites regulate cell signaling and growth via covalent modification of proteins. Dev Cell. 2020;54:156–70.
13. Karmazyn M, Gan XT. Treatment of the cardiac hypertrophic response and heart failure with ginseng, ginsenosides, and ginseng-related products. Can J Physiol Pharmacol. 2017;95:1170–6.
14. Li S, Yu Y, Bian X, Yao L, Li M, Lou YR, et al. Prediction of oral hepatotoxic dose of natural products derived from traditional Chinese medicines based on SVM classifier and PBPK modeling. Arch Toxicol 2021;95:1683–701.
15. Wu W, Jiao C, Li H, Ma Y, Jiao L, Liu S. LC-MS based metabolic and metabonomic studies of Panax ginseng. Phytochem Anal. 2018;29:331–40.
16. Kim JH. Pharmacological and medical applications of Panax ginseng and ginsenosides: a review for use in cardiovascular diseases. J Ginseng Res. 2018;42:264–9.
17. Shi ZY, Zeng JZ, Wong AST. Chemical structures and pharmacological profiles of ginseng saponins. Molecules 2019;24:2443.
18. Liu X, Mi X, Wang Z, Zhang M, Hou J, Jiang S, et al. Ginsenoside Rg3 promotes regression from hepatic fibrosis through reducing inflammation-mediated autophagy signaling pathway. Cell Death Dis. 2020;11:454.
19. Tang M, Bian W, Cheng L, Zhang L, Jin R, Wang W, et al. Ginsenoside Rg3 inhibits keloid fibroblast proliferation, angiogenesis and collagen synthesis in vitro via the TGF-β/Smad and ERK signaling pathways. Int J Mol Med. 2018;41:1487–99.
20. Wang M, Chen L, Liu D, Chen H, Tang DD, Zhao YY. Metabolomics highlights pharmacological bioactivity and biochemical mechanism of traditional Chinese medicine. Chem Biol Interact. 2017;273:133–41.
21. Wang Y, Wang J, Yao M, Zhao X, Fritsche J, Schmitt-Kopplin P, et al. Metabonomics study on the effects of the ginsenoside Rg3 in a beta-cyclodextrin-based formulation on tumor-bearing rats by a fully automatic hydrophilic interaction/reversed-phase column-switching HPLC-ESI-MS approach. Anal Chem. 2008;80:4680–8.
22. Miao H, Cao G, Wu XQ, Chen YY, Chen DQ, Chen L, et al. Identification of endogenous 1-aminopyrene as a novel mediator of progressive chronic kidney disease via aryl hydrocarbon receptor activation. Br J Pharmacol. 2020;177:3415–35.
23. Chen DQ, Cao G, Chen H, Argyopoulos CP, Yu H, Su W, et al. Identification of serum metabolites associating with chronic kidney disease progression and anti-fibrotic effect of 5-methoxytryptophan. Nat Commun. 2019;10:1476.
24. Feng YL, Cao G, Chen DQ, Vaziri ND, Chen L, Zhang J, et al. Microbiome-metabolomics reveals gut microbiota associated with glycine-conjugated metabolites and polyamine metabolism in chronic kidney disease. Cell Mol Life Sci. 2019;76:4961–78.
25. Wang X, Zhang A, Yan G, Sun W, Han Y, Sun H. Metabolomics and proteomics annotate therapeutic properties of geniposide: targeting and regulating multiple perturbed pathways. PLoS One. 2013;8:e71403.
26. Gu Y, Zhang Y, Shi X, Li X, Hong J, Chen J, et al. Effect of traditional Chinese medicine berberine on type 2 diabetes based on comprehensive metabonomics. Talanta. 2010;81:766–72.
27. Lai Q. Study on the dynamic syndrome transformation characteristics of "from deficiency to stasis" and the characteristics of traditional Chinese medicine prescription and syndrome [D]. China Pharmaceutical University, 2020.
28. Gao E, Lei YH, Shang X, Huang ZM, Zuo L, Boucher M, et al. A novel and efficient model of coronary artery ligation and myocardial infarction in the mouse. Circ Res. 2010;107:1445–53.
29. Morris J, Dunham A. Metoprolol. In: StatPearls [Internet]. Treasure Island (FL): (StatPearls Publishing; 2021) PMID: 30422518.
30. Lobo-Gonzalez M, Galán-Arriola C, Rossello X, González-Del-Hoyo M, Vilchez JP, Higuero-Verdejo MI, et al. Metoprolol blunts the time-dependent progression of infarct size. Basic Res Cardiol. 2020;115:55.
31. Qi J, Tan Y, Fan D, Pan W, Yu J, Xu W, et al. Songling Xuemaikang Capsule inhibits isoproterenol-induced cardiac hypertrophy via CaMKIIδ and ERK1/2 pathways. J Ethnopharmacol. 2020;253:112660.
32. Lorca R, Jiménez-Blanco M, García-Ruiz JM, Pizarro G, Fernández-Jiménez R, García-Álvarez A, et al. Coexistence of transmural and lateral wavefront progression of myocardial infarction in the human heart. Rev Esp Cardiol (Engl Ed). 2021;74:870–7.
33. Lai Q, Yuan G, Shen L, Zhang L, Fu F, Liu Z, et al. Oxoeicosanoid receptor inhibition alleviates acute myocardial infarction through activation of BCAT1. Basic Res Cardiol. 2021;116:3.
34. Ma D, Zheng B, Du H, Han X, Zhang X, Zhang J, et al. The mechanism underlying the protective effects of tannic acid against isoproterenol-induced myocardial fibrosis in mice. Front Pharmacol. 2020;11:716.
35. Fan Q, Tao R, Zhang H, Xie H, Lu L, Wang T, et al. Dectin-1 contributes to myocardial ischemia/reperfusion injury by regulating macrophage polarization and neutrophil infiltration. Circulation. 2019;139:663–78.
36. Lang M, Ou D, Liu Z, Li Y, Zhang X, Zhang F. LncRNA MHRT promotes cardiac fibrosis via miR-3185 pathway following myocardial infarction. Int Heart J. 2021;62:891–9.
37. Zhang QJ, He Y, Li Y, Shen H, Lin L, Zhu M, et al. Matricellular protein Cilp1 promotes myocardial fibrosis in response to myocardial infarction. Circ Res. 2021;129:1021–1035.
38. Lai Q, Yuan GY, Wang H, Liu ZL, Kou JP, Yu BY, et al. Exploring the protective effects of schizandrol A in acute myocardial ischemia mice by comprehensive metabolomics profiling integrated with molecular mechanism studies. Acta Pharmacol Sin. 2020;41:1058–72.
39. Zhou K, Ding X, Yang J, Hu Y, Song Y, Chen M, et al. Metabolomics reveals metabolic changes caused by low-dose 4-Tert-Octylphenol in mice liver. Int J Environ Res Public Health. 2018;15:2686.
40. Carrola J, Rocha CM, Barros AS, Gil AM, Goodfellow BJ, Carreira IM, et al. Metabolic signatures of lung cancer in biofluids: NMR-based metabonomics of urine. J Proteome Res. 2011;10:221–30.
41. Bradford BU, O'Connell TM, Han J, Kosyk O, Shymonyak S, Ross PK, et al. Metabolomic profiling of a modified alcohol liquid diet model for liver injury in the mouse uncovers new markers of disease. Toxicol Appl Pharmacol. 2008;232:236–43.
42. Sass JO, Mohr V, Olbrich H, Engelke U, Horvath J, Fliegauf M, et al. Mutations in ACY1, the gene encoding aminoacylase 1, cause a novel inborn error of metabolism. Am J Hum Genet. 2006;78:401–9.

43. Yu B, Liu X, Cao X, Zhang M, Chang H. Study of the expression and function of ACY1 in patients with colorectal cancer. Oncol Lett. 2017;13:2459–64.
44. Shi H, Hayes MT, Kirana C, Miller RJ, Keating JP, Stubbs RS. Overexpression of aminoacylase 1 is associated with colorectal cancer progression. Hum Pathol. 2013;44:1089–97.
45. Wei X, Li J, Xie H, Ling Q, Wang J, Lu D, et al. Proteomics-based identification of the tumor suppressor role of aminoacylase 1 in hepatocellular carcinoma. Cancer Lett. 2014;351:117–25.
46. Zhong Y, Onuki J, Yamasaki T, Ogawa O, Akatsuka S, Toyokuni S. Genome-wide analysis identifies a tumor suppressor role for aminoacylase 1 in iron-induced rat renal cell carcinoma. Carcinogenesis. 2009;30:158–64.
47. Fujioka T, Kühn A, Sanchez-Martinez S, Bijnens BH, Hui W, Slorach C, et al. Impact of interventricular interactions on left ventricular function, stroke volume, and exercise capacity in children and adults with ebstein's anomaly. JACC Cardiovasc Imaging. 2019;12:925–7.
48. Aimo A, Gaggin HK, Barison A, Emdin M, Januzzi JL Jr. Imaging, biomarker, and clinical predictors of cardiac remodeling in heart failure with reduced ejection fraction. JACC Heart Fail. 2019;7:782–94.
49. Cunningham JW, Claggett BL, O'Meara E, Prescott MF, Pfeffer MA, Shah SJ, et al. Effect of sacubitril/valsartan on biomarkers of extracellular matrix regulation in patients with HFpEF. J Am Coll Cardiol. 2020;76:503–14.
50. McLaughlin S, McNeill B, Podrebarac J, Hosoyama K, Sedlakova V, Cron G, et al. Injectable human recombinant collagen matrices limit adverse remodeling and improve cardiac function after myocardial infarction. Nat Commun. 2019;10:4866.
51. Rusu M, Hilse K, Schuh A, Martin L, Slabu I, Stoppe C, et al. Biomechanical assessment of remote and postinfarction scar remodeling following myocardial infarction. Sci Rep. 2019;9:16744.
52. Friebel J, Weithauser A, Witkowski M, Rauch BH, Savvatis K, Dörner A, et al. Protease-activated receptor 2 deficiency mediates cardiac fibrosis and diastolic dysfunction. Eur Heart J. 2019;40:3318–32.
53. Trippel TD, Van Linthout S, Westermann D, Lindhorst R, Sandek A, Ernst S, et al. Investigating a biomarker-driven approach to target collagen turnover in diabetic heart failure with preserved ejection fraction patients. Effect of torasemide versus furosemide on serum C-terminal propeptide of procollagen type I (DROP-PIP trial). Eur J Heart Fail. 2018;20:460–70.
54. Chiang MH, Liang CJ, Lin LC, Yang YF, Huang CC, Chen YH, et al. miR-26a attenuates cardiac apoptosis and fibrosis by targeting ataxia-telangiectasia mutated in myocardial infarction. J Cell Physiol. 2020;235:6085–102.
55. Frangogiannis NG. Cardiac fibrosis. Cardiovasc Res. 2021;117:1450–88.
56. Miller YE, Minna JD, Gazdar AF. Lack of expression of aminoacylase-1 in small cell lung cancer. Evidence for inactivation of genes encoded by chromosome 3p. J Clin Invest. 1989;83:2120–4.
57. Oatmen KE, Cull E, Spinale FG. Heart failure as interstitial cancer: emergence of a malignant fibroblast phenotype. Nat Rev Cardiol. 2020;17:523–31.
58. Ren B, Feng J, Yang N, Guo Y, Chen C, Qin Q. Ginsenoside Rg3 attenuates angiotensin II-induced myocardial hypertrophy through repressing NLRP3 inflammasome and oxidative stress via modulating SIRT1/NF-κB pathway. Int Immunopharmacol. 2021;98:107841.
59. Titus VH, Cowling AS, Kailasam RT. S. Collagen receptor cross-talk determines α-smooth muscle actin-dependent collagen gene expression in angiotensin II-stimulated cardiac fibroblasts. J Biol Chem. 2019;294:19723–39.
60. Zile MR, O'Meara E, Claggett B, Prescott MF, Solomon SD, Swedberg K, et al. Effects of sacubitril/valsartan on biomarkers of extracellular matrix regulation in patients with HFrEF. J Am Coll Cardiol. 2019;73:795–806.